

Intense X-ray Vortices Generation via Wavefront Shaping in high-gain Free-Electron Lasers

Zhikai Zhou,¹ Yin Kang,^{2,3} Weishi Wan,¹ and Chao Feng^{4,*}

¹*ShanghaiTech University, Shanghai 201210, China*

²*Shanghai Institute of Applied Physics, Chinese Academy of Sciences, Shanghai 201800, China*

³*University of Chinese Academy of Sciences, Beijing 100049, China*

⁴*Shanghai Advanced Research Institute, Chinese Academy of Sciences, Shanghai 201210, China*

The x-ray vortex optical beam, distinguished by its topological charge and orbital angular momentum, offers new insights in probing complex electronic structures, enhancing material characterization, and advancing high-resolution imaging techniques. Here we propose a straightforward and effective method to generate intense x-ray vortices with tunable wavelengths in high-gain free-electron lasers (FELs). By simply adjusting the wavefront tilt of the radiation pulse during the FEL gain process, high-quality vortex beam can be amplified until saturation. Compared to existing methods for FEL vortex generation, the proposed technique imposes no wavelength limitations and can be easily implemented in high-gain FEL facilities, regardless of the operation modes.

The rapid development of vortex optical beams carrying orbital angular momentum (OAM) [1, 2] in conventional laser fields has led to numerous significant applications, including optical tweezers [3–6], super-resolution imaging [7–10], and quantum information processing [11]. These beams are distinguished by their unique helical phase structure, characterized by a phase singularity and an azimuthal phase dependence $e^{-il\phi}$, where l represents the topological charge indicating the number of times that vortex beam twists in one wavelength, and ϕ is the azimuthal angle. The intense potential of this specific property to transform various fields, from fundamental physics to material science and biology, has generated considerable interest [12–15]. Extending OAM technology to the x-ray regime, which could offer unprecedented insights into nanoscale structures and dynamics, is particularly enticing [16–20]. However, conventional laser-based methods are often limited by their inability to achieve the short wavelengths required for x-ray production.

Modern free-electron lasers (FELs) have emerged as one of the most promising avenues for generating coherent x-ray sources with high intensity. The advent of FELs has represented a paradigm shift in x-ray science, providing ultrahigh brightness, femtosecond to attosecond pulse durations, and tunability across a broad spectral range [21–30]. These attributes make FELs particularly suitable for investigating x-ray OAM. One pioneering approach to generate OAM in FELs focuses on using helical undulators, which naturally produce higher harmonics carrying OAM due to the helical trajectory of electrons within the undulator’s magnetic field [31, 32]. However, this method often results in relatively weak OAM signals at the fundamental wavelength [33]. To address this issue, a more elaborate technique has been developed, involving the interaction of a seed laser with an electron beam in a helical undulator, enabling the generation of vortex beams at the fundamental frequency. Additionally, clever methods of using seed lasers with tailored

transverse phases to shape electron bunches into helical patterns, thus radiating OAM light, have been explored [34–38]. Although these methods show promise, they are frequently constrained by the availability and quality of seed lasers and optical elements, and often lack broad wavelength tunability. Furthermore, achieving precise control over the electron beam’s microstructure and maintaining the dominance of the OAM mode throughout the FEL amplification process remains a significant technical challenge.

In this letter, we propose a novel method for generating intense x-ray vortex beams via mode conversion in high-gain FELs. Our approach leverages the natural amplification process of FELs to produce high-quality OAM beams with tunable wavelengths. This technique offers several advantages over existing methods, including the absence of wavelength limitations and the ease of implementation in existing high-gain FEL facilities.

The key to the proposed method is subtly adjusting the wavefront of the radiation pulse during the FEL amplification process, leveraging diffraction effects and the FEL gain to continually twist the radiation profile into a vortex beam at saturation. The schematic layout of the proposed technique is shown in Fig. 1, where the self-amplified spontaneous emission (SASE) mode is adopted as an example to demonstrate the physical process [39, 40]. Similar to the self-seeding technique, the undulator is separated into two parts by a bypass chicane, as shown in Fig. 1(a). After sufficient amplification in the SASE undulator, the FEL pulse and the electron beam are separated in the chicane, and the transverse phase of the radiation pulse is shaped before it serves as a seed in the following output undulator.

There are three optical elements in the chicane: a concave mirror to reflect the input FEL beam and adjust its position, a wavefront tilt reflector to slightly tune the wavefront tilt to shape the transverse pattern of the FEL beam, and another concave mirror to focus the output FEL beam and direct it into the following undulator.

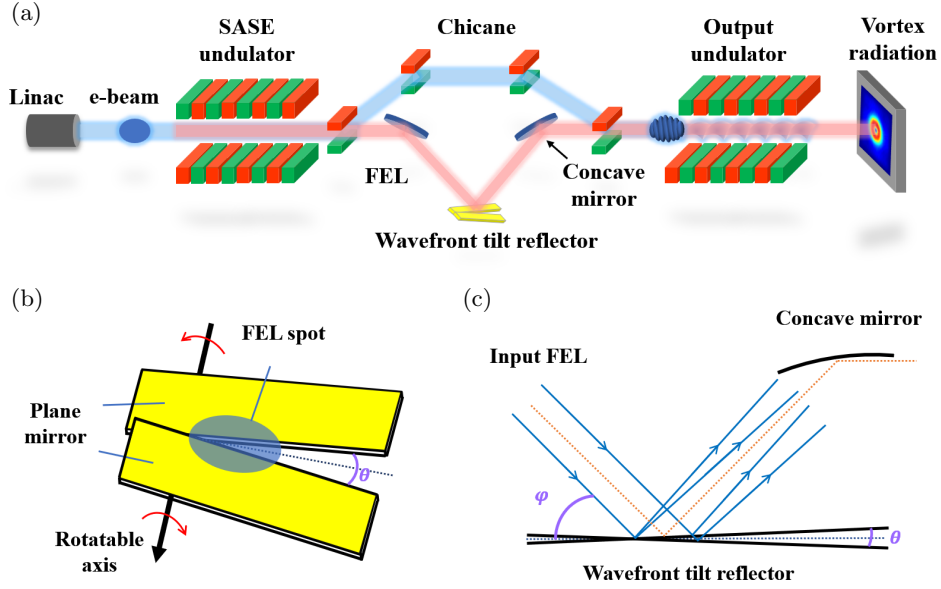


FIG. 1. Diagram for the proposed method. (a) Schematic layout for x-ray OAM generation based on SASE. (b) The structure of the wavefront tilt reflector. (c) Two-dimensional schematic graph of the optical propagation of the FEL pulse in the chicane.

The wavefront tilt reflector consists of two plane mirrors that can be independently rotated around the same axis. The angle between the two mirrors is denoted as θ , as shown in Fig. 1(b). We assume that θ is very small and negligible compared to the incidence angle φ of the FEL beam. The input FEL pulse should be centrally positioned between these two plane mirrors, creating different wavefront tilts in the two halves of the FEL spot after reflection, as shown in Fig. 1(c).

The transverse phase of the output FEL pulse will be shaped due to the different optical path length. For a given position x from the rotatable axis (along the dividing line of the two mirrors), the optical path difference Δl can be represented as

$$\Delta l = \frac{2x \tan(\theta/2)}{\sin \varphi}. \quad (1)$$

Consequently, the variation of the transverse phase $\Delta\phi$ can be expressed as $\Delta\phi = 2\pi\Delta l/\lambda$, where λ is the central wavelength of the FEL. The phase variation in the two halves of the FEL spot can be expressed as:

$$\Delta\phi = \begin{cases} \frac{2\pi x \tan(\theta/2)}{\lambda \sin \varphi}, \\ \frac{2\pi x \tan(\theta/2)}{\lambda \sin \varphi}. \end{cases} \quad (2)$$

For a given optical spot projection size σ of the FEL beam along the dividing line, only a portion of the spot with a diameter of d will interact with the electron beam in the following undulator. To achieve optical vortex radiation with a topological charge of 1 or -1, the transverse phase variation in d should be around 2π or -2π . Hence, the required absolute tilt angle of the wavefront tilt reflector

can be represented as

$$\theta = \arctan\left(\frac{\lambda \sin \varphi}{d}\right). \quad (3)$$

When the wavelength of the input laser changes, the tilt angle can be adjusted accordingly to maintain a constant optical transverse phase. For an input FEL pulse with a central wavelength of 5 nm, an incidence angle φ of 175 mrad, and an interaction range d of approximately 100 μm , the required θ is calculated to be about 8.7 μrad to cover the transverse phase variation interval from 0 to 2π .

The x-ray transport process through the concave mirror can be studied using the wave optical propagation method [41, 42]. After the concave mirror with a focal length of f , the complex optical field of the radiation $\tilde{E}(x_1, y_1)$ will be changed to

$$\tilde{E}'(x_1, y_1) = \tilde{E}(x_1, y_1) e^{-\frac{ik}{2f}(x_1^2 + y_1^2)}, \quad (4)$$

where k denotes the wavenumber of the FEL pulse. The optical field after a propagating distance f can be derived from Fresnel optics as

$$E(x, y) = \frac{e^{ikf}}{i\lambda f} e^{\frac{ik}{2f}(x^2 + y^2)} \times \mathcal{F}[\tilde{E}'(x_1, y_1) e^{\frac{ik}{2f}(x_1^2 + y_1^2)}], \quad (5)$$

and it can be mathematically simplified to

$$E(x, y) = \frac{e^{ikf}}{i\lambda f} e^{\frac{ik}{2f}(x^2 + y^2)} \times \mathcal{F}[\tilde{E}(x_1, y_1)]. \quad (6)$$

Eq. 6 indicates that the optical field in the focal plane is the Fourier transformation of the initial field, preserv-

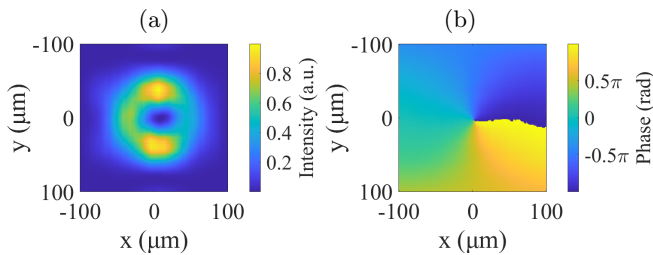


FIG. 2. The intensity (a) and the phase (b) distributions of the output FEL after the chicane.

ing its phase structure. With a focal length of approximately 3 m for the second concave mirror, the transverse intensity and phase of the FEL pulse in the focal plane are depicted in Fig. 2(a) and (b), respectively. As shown in Fig. 2(b), the phase of the output FEL pulse resembles that described by Eq. 2. The upper and lower halves exhibit oppositely directed wavefront tilts, resulting in a hollow structure in the radiation intensity distribution, as illustrated in Fig. 2(a). Due to the small diffraction angle of the x-ray beam, the transverse distribution of the output FEL beam generally follows this pattern before interacting with the electron beam in the subsequent undulator.

To demonstrate the feasibility of this method for initiating coherent x-ray OAM radiation, three-dimensional simulations using GENESIS [43] were conducted, utilizing typical parameters for a soft X-ray FEL facility, as summarized in Table I. The SASE undulator contains of five undulator segments, and the FEL peak power exceeds 3 GW at the end of the SASE undulator. Subsequently, both the electron beam and the SASE beam were then sent into the chicane. The propagation of the SASE beam was simulated using the wave optical propagation method with same optical parameters as described earlier. Here we assume a power reflectivity of 80% for each mirror. The shaped radiation beam was then sent into the following undulator to interact with the same electron beam. The microbunching in the electron beam, formed in the previous SASE undulator, was dispersed after passing through the chicane.

TABLE I. Main parameters used in simulations.

Parameters	Value
Electron beam energy	2.5 GeV
Peak current	3000 A
Bunch length	80 fs
Emittance	0.5 mm·mrad
Undulator period	4 cm
Undulator segment length	4 m
Radiation wavelength	5 nm

The output undulator is resonant at the same wavelength as the SASE undulator. At the entrance of the

undulator, the radiation pulse interacts with the electron beam, creating wavefront tilt microbunchings. Consequently, the evolution of the radiation profile is primarily influenced by diffraction, resulting in no power increase in the first 2 meters, as depicted in Fig. 3(a). The initial radiation wavefront does not match the characteristics of a guided FEL mode exhibiting a Gaussian intensity distribution, leading to a twisting of the transverse pattern due to diffraction and amplification within the output undulator, which produces helical microbunchings.

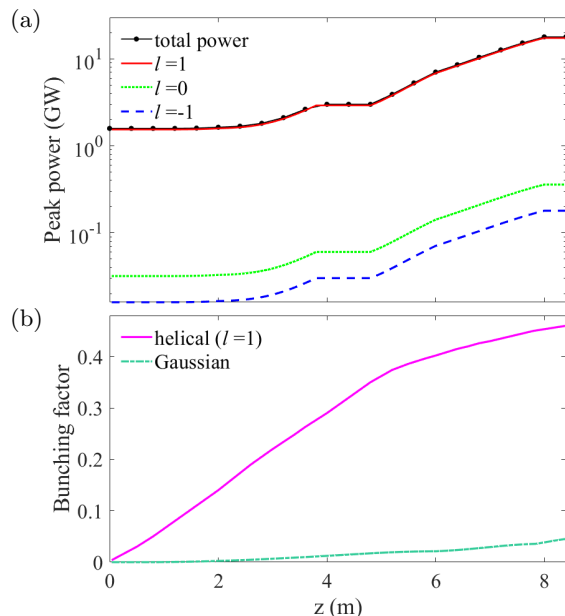


FIG. 3. Gain curves (a) and evolutions of bunching factors (b) for different FEL modes along the output undulator.

The microbunching can be quantified by the bunching factor, $b^l(k) = |\langle e^{-iks - il\phi} \rangle|$, where the bracket denotes averaging over all coordinates, and s is the longitudinal position along the electron beam [24]. As shown in Fig. 3(b), the helical bunching factor grows from 0 to over 0.1 within the first 2 meters of the output undulator. As a result, the intensity and phase of the radiation field begin to twist, as illustrated in the first line of Fig. 4. Following this, the FEL enters a high-gain regime where the selection of transverse modes tends to favor lower-order modes, such as the Gaussian mode ($l = 0$) and the OAM mode with $l = 1$.

Typically, in this regime, with a sufficiently long undulator, the Gaussian mode, which has the highest growth rate, is generally the sole mode at saturation. However, the application of wavefront shaping during the gain process allows diffraction to enhance the OAM mode, facilitating its saturation much earlier than the Gaussian mode. As higher modes with reduced growth rates are eliminated, the amplification process ultimately culminates in a predominance of the guided OAM mode with $l = 1$ at saturation, as illustrated in Fig. 3(a). The FEL

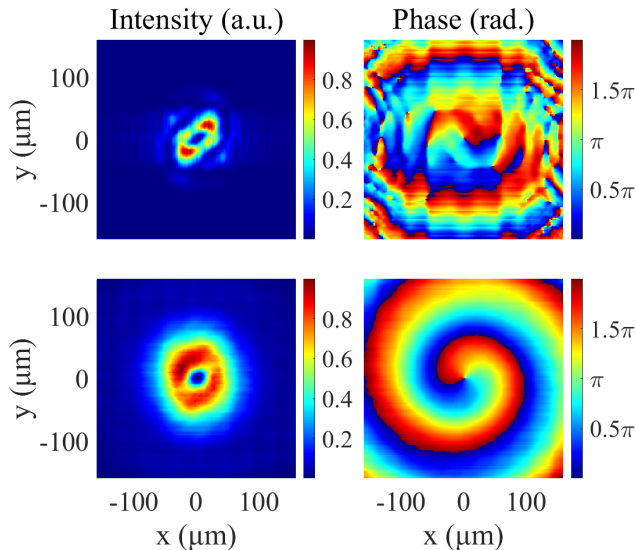


FIG. 4. Intensity and phase profiles after 2 m of the output undulator (upper line), and at the exit of output undulator (lower line).

peak power reaches tens of gigawatts at the exit of the output undulator, where the ratio of the $l = 1$ mode is 97%, while that for Gaussian mode is only 2%. The characteristic hollow intensity distribution and helical phase of the vortex radiation at saturation are illustrated in the second line of Fig. 4.

The underlying physics of the proposed method involves inducing wavefront tilts in opposite directions on either half of the FEL spot to facilitate the rotation of the radiation phase front. In the previous design, the angle of the wavefront tilt reflector was determined according to Eq. 3. Deviations from the ideal value will not affect the trend of vortex formation but will influence the position of the optical singularity, thereby impacting the transverse symmetry of the output FEL vortex. Consequently, it is essential to analyze the adjustment precision of the wavefront tilt reflector. Multiple tests indicate that deviations should be controlled within 10%, approximately $0.87 \mu\text{rad}$ in this context, to ensure optimal vortex quality. If the tilt angles exceed this threshold, the hollow intensity distribution of the optical OAM will be compromised, as shown in Fig. 5, although the phase structure may still be well-maintained. To achieve shorter wavelength vortex beams, stricter requirements for wavefront tilt adjustment precision will be necessary, necessitating careful design of the mechanical system of the x-ray beamline.

In conclusion, we have proposed a novel method to generate FEL vortices with variable wavelengths. By slightly adjusting the wavefront of the radiation pulse during the FEL gain process, the OAM mode can dominate and be amplified until saturation. This method is particularly

well-suited for FEL facilities with the self-seeding setup, which naturally incorporates the necessary chicane and optical transport systems required by this approach. For applications in the hard x-ray regime, it may be essential to employ crystal transmission or reflection to achieve the required wavefront tilt. The proposed method can also be applied in the seed laser system of an external seeded FEL to control the transverse profile of the coherent high-harmonic radiation. Currently, this method is limited to generate vortex beams with topological charges of 1 and -1. However, we are actively exploring ways to extend its capabilities to produce vortices with higher topological charges through wavefront manipulation. The proposed method is not only compatible with various operational modes of FELs but also promises to deliver x-ray vortex beams of unprecedented intensity and quality, paving the way for groundbreaking research in x-ray sciences.

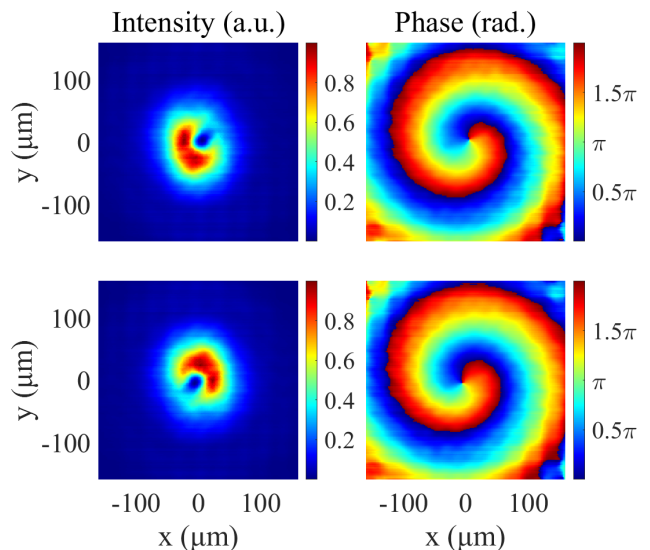


FIG. 5. Adjustment precision analysis for the wavefront tilt reflector. Intensity and phase profiles with an angle deviation of -5% (upper line) and +5% (lower line).

The authors would like to thank Hao Sun, Kaiqing Zhang, Yiwen Liu and Zhentang Zhao for helpful discussions. This work was supported by the National Natural Science Foundation of China (12122514, 12435011), CAS Project for Young Scientists in Basic Research (YSBR-115), and Strategic Priority Program of the CAS (XDB0530300)

* fengc@sari.ac.cn

- [1] L. Allen, M. W. Beijersbergen, R. J. C. Spreeuw, and J. P. Woerdman, *Phys. Rev. A* **45**, 8185 (1992).
- [2] Y. Shen, X. Wang, Z. Xie, C. Min, X. Fu, Q. Liu, M. Gong, and X. Yuan, *Light: Science & Applications*

- 8**, 90 (2019).
- [3] L. Paterson, M. P. MacDonald, J. Arlt, W. Sibbett, P. E. Bryant, and K. Dholakia, *Science* **292**, 912 (2001).
- [4] M. P. MacDonald, L. Paterson, K. Volke-Sepulveda, J. Arlt, W. Sibbett, and K. Dholakia, *Science* **296**, 1101 (2002).
- [5] D. G. Grier, *Nature* **424**, 810 (2003).
- [6] Z. Shen, Z. J. Hu, G. H. Yuan, C. J. Min, H. Fang, and X.-C. Yuan, *Opt. Lett.* **37**, 4627 (2012).
- [7] M. Erhard, R. Fickler, M. Krenn, and A. Zeilinger, *Light: Science & Applications* **7**, 17146 (2018).
- [8] S. Fürhapter, A. Jesacher, S. Bernet, and M. Ritsch-Marte, *Opt. Express* **13**, 689 (2005).
- [9] F. Tamburini, G. Anzolin, G. Umbriaco, A. Bianchini, and C. Barbieri, *Phys. Rev. Lett.* **97**, 163903 (2006).
- [10] E. Nagali, L. Sansoni, F. Sciarrino, F. De Martini, L. Marrucci, B. Piccirillo, E. Karimi, and E. Santamato, *Nature Photonics* **3**, 720 (2009).
- [11] M. Mafu, A. Dudley, S. Goyal, D. Giovannini, M. McLaren, M. J. Padgett, T. Konrad, F. Petruccione, N. Lütkenhaus, and A. Forbes, *Phys. Rev. A* **88**, 032305 (2013).
- [12] W. J. Firth and D. V. Skryabin, *Phys. Rev. Lett.* **79**, 2450 (1997).
- [13] X. Zhuang, *Science* **305**, 188 (2004).
- [14] S. B. Wang and C. T. Chan, *Nature Communications* **5**, 3307 (2014).
- [15] Y. Zhao, A. N. Askarpour, L. Sun, J. Shi, X. Li, and A. Alù, *Nature Communications* **8**, 14180 (2017).
- [16] Y. Takahashi, A. Suzuki, S. Furutaku, K. Yamauchi, Y. Kohmura, and T. Ishikawa, *Phys. Rev. B* **87**, 121201 (2013).
- [17] C. Hernández-García, J. Vieira, J. T. Mendonça, L. Rego, J. San Román, L. Plaja, P. R. Ribic, D. Gauthier, and A. Picón, *Photonics* **4**, 10.3390/photonics4020028 (2017).
- [18] G. De Ninno *et al.*, *Nature Photonics* **14**, 554 (2020).
- [19] B. Wang, N. J. Brooks, P. Johnsen, N. W. Jenkins, Y. Esashi, I. Binnie, M. Tanksalvala, H. C. Kapteyn, and M. M. Murnane, *Optica* **10**, 1245 (2023).
- [20] M. R. McCarter, L. E. D. Long, J. T. Hastings, and S. Roy, *Journal of Physics: Condensed Matter* **36**, 423003 (2024).
- [21] W. Ackermann *et al.*, *Nature Photonics* **1**, 336 (2007).
- [22] P. Emma *et al.*, *Nature Photonics* **4**, 641 (2010).
- [23] T. Ishikawa *et al.*, *Nature Photonics* **6**, 540 (2012).
- [24] E. Allaria *et al.*, *Journal of Synchrotron Radiation* **22**, 485 (2015).
- [25] H.-S. Kang, C.-K. Min, H. Heo, C. Kim, H. Yang, G. Kim, I. Nam, S. Y. Baek, H.-J. Choi, G. Mun, *et al.*, *Nature Photonics* **11**, 708 (2017).
- [26] W. Decking *et al.*, *Nature Photonics* **14**, 391 (2020).
- [27] E. Prat *et al.*, *Nature Photonics* **14**, 748 (2020).
- [28] C. Feng, T. Liu, S. Chen, K. Zhou, K. Zhang, Z. Qi, D. Gu, Z. Wang, Z. Jiang, X. Li, *et al.*, *Optica* **9**, 785 (2022).
- [29] P. K. Maroju, C. Grazioli, M. Di Fraia, M. Moioli, D. Ertel, H. Ahmadi, O. Plekan, P. Finetti, E. Allaria, L. Giannessi, *et al.*, *Nature* **578**, 386 (2020).
- [30] J. Duris, S. Li, T. Driver, E. G. Champenois, J. P. MacArthur, A. A. Lutman, Z. Zhang, P. Rosenberger, J. W. Aldrich, R. Coffee, *et al.*, *Nature Photonics* **14**, 30 (2020).
- [31] E. Hemsing, P. Musumeci, S. Reiche, R. Tikhoplav, A. Marinelli, J. B. Rosenzweig, and A. Gover, *Phys. Rev. Lett.* **102**, 174801 (2009).
- [32] E. Hemsing, A. Marinelli, and J. B. Rosenzweig, *Phys. Rev. Lett.* **106**, 164803 (2011).
- [33] G. Geloni, E. Saldin, E. Schneidmiller, and M. Yurkov, *Nucl. Instrum. Methods Phys. Res. Sec. A: Accel. Spectrom. Detect. Assoc. Equip.* **581**, 856 (2007).
- [34] E. Hemsing and A. Marinelli, *Phys. Rev. Lett.* **109**, 224801 (2012).
- [35] P. c. v. R. Ribič, D. Gauthier, and G. De Ninno, *Phys. Rev. Lett.* **112**, 203602 (2014).
- [36] P. c. v. Rebernik Ribič, B. Rösner, D. Gauthier, E. Allaria, F. Döring, L. Foglia, L. Giannessi, N. Mahne, M. Manfreda, C. Masciovecchio, *et al.*, *Phys. Rev. X* **7**, 031036 (2017).
- [37] H. Sun, X. Wang, C. Feng, L. Tu, W. Fan, and B. Liu, *High Power Laser Science and Engineering* **9**, e65 (2021).
- [38] J. Yan and G. Geloni, *Advanced Photonics Nexus* **2**, 036001 (2023).
- [39] A. M. Kondratenko and E. L. Saldin, in *Generating of coherent radiation by a relativistic electron beam in an undulator* (1980).
- [40] R. Bonifacio, C. Pellegrini, and L. Narducci, *Optics Communications* **50**, 373 (1984).
- [41] J. W. Goodman, in *Introduction to Fourier optics* (Roberts and Company, 1969).
- [42] S. Serkez, J. Krzywinski, Y. Ding, and Z. Huang, *Phys. Rev. ST Accel. Beams* **18**, 030708 (2015).
- [43] S. Reiche, *Nucl. Instrum. Methods Phys. Res. Sec. A: Accel. Spectrom. Detect. Assoc. Equip.* **429**, 243 (1999).